Austrian Journal of Earth Sciences | Volume 98 | 106 - 119 | Vienna | 2005

Palaeoclimate background and stratigraphic evidence of Late Norian / Early Rhaetian polyphase synsedimentary tectonics in the Hallstatt Limestones of Berchtesgaden (Rappoltstein, Southern Germany)

Thomas HORNUNG

KEYWORDS

polyphase synsedimentary tectonics
Hallstatt Limestones
"ammonite rudstone"
palaeotemperatures
stable isotopes
Late Triassic

Institute for Geology & Palaeontology, Innrain 52, University of Innsbruck, A-6020 Innsbruck.
Email: thomas.hornung@uibk.ac.at

Abstract

A short succession of thick-bedded Hallstatt Limestones (Juvavic Nappe, central Northern Calcareous Alps) with two generations of synsedimentary fissures and five stages of sedimentation (S1 to S5) is described from the northwestern edge of the Rappoltstein block (Berchtesgaden Mountains, Southern Germany). The normally bedded sequence consisting of grey and red tinted bioclastic wacke- and packstones, contains three fissures metre-sized in length and width, and filled with an "ammonite rudstone" (Krystyn, 1991) consisting mainly of *Cochloceras* sp. and *Arcestes* sp. The diachroneity between sediment and fissure-fillings is evidenced by two different conodont assemblages and one ammonite assemblage: a nearly monospecific presence of *Norigondolella steinbergensis* with rare *Epidondollela* ex gr. *bidentata* in the thick-bedded bioclastic limestones points approximately to the E. *bidentata* conodont assemblage zone (A.Z.) / *quinquepunctatus* ammonite zone representing Sevatian 1; S1). Rare *Misikella hernsteini* and *Epigondolella* ex. gr. *bidentata* found in two of the three fissures indicate Sevatian II (*hernsteini* conodont A.Z.; S2). Fissure 1 is bordered by radial-fibrous cements indicating long-term submarine exposure (S3). A macrofossil assemblage of abundant *Cochloceras* sp. found in its sedimentary infill implies an Early Rhaetian age (S4). Thin fractures filled with grey mudstones, crossing fissure 1, indicate a fifth phase of sedimentation (S5) at the very end of the Hallstatt Limestone development. Stable isotope values obtained from whole rock samples (oxygen and carbon, V-PDB) and calcium-apatite of conodonts (oxygen, V-SMOW) provide supplementary information about palaeotemperatures. Assuming that open marine Triassic seawater $\delta^{18}O$ values were close to -1 ‰ V-SMOW (for ice-free periods), calculations result in low temperatures of approximately 12-13° C: If the Hallstatt Basin was as shallow as suggested by earlier studies, the temperatures would be too low to be within the range of tolerance of co-existing reef-building corals growing on the adjacent carbonate platforms.

Vom nordwestlichen Rappoltstein nahe Berchtesgaden / Süddeutschland wird eine Hallstätter Kalkabfolge (Juvavisches Deckensystem, Zentrale Nördliche Kalkalpen) mit synsedimentären Spalten und wenigstens fünf unterschiedlichen Sedimentationsaltern (S1 – S5) beschrieben. In eine hangparallel nach Norden einfallende, dickbankige und makrofossilarme grau-rötliche Kalkserie sind drei Spalten eingelagert, die sich durch eine satt-rötliche Sedimentfärbung, aber auch durch reiches Vorkommen von *Cochloceras* sp. und *Arcestes* sp. vom umgebenden Sediment abheben („Ammoniten-Rudstone" als Spalten-Konzentratlagerstätte sensu Krystyn, 1991). Unterschiedliche Ammoniten- und Conodonten-Alter aus Umgebungs- versus Spaltensediment ergeben eine deutliche zeitliche Diskrepanz: Beinahe monospezifisch auftretende *Norigondolella steinbergensis* mit seltenen *Epigondolella* ex. gr. *bidentata* aus dem umgebenden „Normalsediment" zeigen frühsevatisches Alter (*bidentata* Conodonten-Zone, *quinquepunctatus* Ammoniten-Zone, Sevat 1, S1), während das seltene Vorkommen von *Misikella hernsteini* in zwei Spaltenfüllungen von „Ammoniten-Rudstones" jedoch auf Sevat 2 hindeutet (*hernsteini* Conodonten-Zone, Sevat II; S2). Randlich gewachsene radial-fibröse Zementsäume (S3) der im Aufschluss zuoberst gelegenen Spalte 1 weisen auf eine längere Offenlegung mit ausbleibender Sedimentation hin. Ihre rötliche Sedimentfüllung mit sehr häufigem Vorkommen von *Cochloceras* sp. indiziert basales Rhät (S4). Spalte 1 durchschlagende dünne Klüfte, gefüllt mit grauen fossilarmen Mudstones, belegen ein fünftes Sedimentationsalter, welches ins oberste Ende der Hallstätter Kalk-Entwicklung einzustufen ist. Diese zuletzt fünf unterschiedlich alten, biostratigraphisch einstufbaren Sedimente (und Zemente) zeigen die Mehrphasigkeit einer synsedimentär-tektonischen Überprägung des Aufschlusses während der obersten Trias an.

Die Untersuchung stabiler Isotopen aus Karbonatgesteinen (Kohlenstoff und Sauerstoff; V-PDB) und aus Kalzium-Apatit von Conodonten (Sauerstoff; V-SMOW) liefert zusätzliche Daten über Paläotemperaturen. Die Kalkulation der $\delta^{18}O$-Werte mit -1 ‰ V-SMOW für eine vereisungsfreie Obertrias ergab niedrige Paläotemperaturen von 12-13° C. Unter der Annahme neuerer Studien, nach denen das Hallstätter Becken flacher gewesen sein dürfte als bisher angenommen, wären die errechneten Werte zu tief für den Toleranzbereich koexistierender riffbildender Korallen auf den benachbarten, in enger räumlicher Bindung zum Hallstätter Becken stehenden Karbonatplattformen.

1. Introduction – Previous studies

Due to its well-exposed and fossil-rich Hallstatt Limestones, the forested Rappoltstein Mountain near Berchtesgaden (Southern

Germany) has been studied since the 19th century (Schafhäutl 1848; Gümbel 1861; Mojsisovics 1893; Schlosser 1898). Its isolated tectonic position exposing upper Triassic Hallstatt Limestones (Juvavic Nappe), which overly a significantly younger Cretaceous and Jurassic series (Tirolic Nappe), have been interpreted and discussed in several studies: Plöchinger (1955) and Pichler (1963), for instance, dated the Rappoltstein into Carnian and Norian – stratigraphic levels older than Carnian were removed during thrusting over younger Tyrolean series. Krystyn and Schlager (1971) interpreted the Rappoltstein as a NE vergent anticlinal structure including Early Carnian to Late Norian limestones. Owing to the coexistence of *Gladigondolella tethydis* and *Paragondolella excelsa*, Donofrio (1975) enlarged the stratigraphic range to the Late Ladinian (Langobardian).

Despite these large-scaled detailed mappings and investigations, the Rappoltstein location described in this paper seems to have received no consideration in literature. Pichler (1963) noted Upper Carnian fossil locations in the north-eastern part of the Rappoltstein and Lower Norian fossil deposits in its southern part. In their work on Hallstatt fossil deposits, Krystyn and Schlager (1971) re-examined Pichler's Upper Carnian north-eastern location interpreting it as a synsedimentary fissure filled with fossil-enriched biomicrites of Tuvalian age.

The location described herein was found accidentally when trying to locate the Carnian sections described by Donofrio (1975). Already during sampling, a difference between homogenous, macrofossil-poor greyish to red tinted limestones and red-coloured limestones with an abundant macrofauna was obvious. The restricted presence of fossil-rich red limestones and their sharply delimited, bed-cutting occurrence, led to the interpretation of synsedimentary fissures as "fossil-traps" sensu Krystyn et al. (1971). The main constituents are ammonoids of variable size (5 to 150 mm). Aided by adequate biomarkers, and compared to similar Hallstatt Limestone locations in Upper Austria (Krystyn, 1991), the Rappoltstein offers a rare opportunity to study Norian / Rhaetian synsedimentary movements in the Berchtesgaden region.

2. Geological setting

The studied section is situated on the northwestern edge of the Rappoltstein block, about 7.5km NE of Berchtesgaden (Fig. 1; UTM: WGS84, Zone 33; E 355048; N 5283229) and lies very closely to thin and medium bedded grey-coloured limestones of the Cretaceous Schrambach Formation of the Tirolic Nappe. This significant tectonic unconformity resulted from the thrusting of the Hallstatt (= Juvavic) Nappe over Tirolic Mesozoic sequences (for further information see Decker et al., 1987; Frank, 1987; Neubauer, 1994; Schweigl and Neubauer, 1997; Gawlick et al., 1999; Gawlick, 2000; Gawlick and Diersche, 2000; Gawlick and Lein, 1997, 2000; Frisch and Gawlick, 2003). Together with another occurrence of Hallstatt Limestones near the Mehlweg and Barmsteine (see fig. 1b), the Rappoltstein forms the northern part of the Dürrnberg Juvavic block area.

The studied section consists of approximately 4 metres of thick-bedded limestones (thickness per bed max. 1.5 m) sharply incised by synsedimentary fissures (Fig. 3). The lithological differentiation is obvious (Fig. $2a_1$): The normal and planar bedded limestones are tinted grey and red and contain only rare macrofossils, the fissure fillings show a red colouring and abundant macrofossils, predominantly ammonoids and crinoid stem ossicles (Fig. $2a_2$). The succession is dissected by vertical dipping normal faults (Figs. 3a, b). The displacement along the faults amounts to a few metres.

The NW Rappoltstein location is bordered by Cretaceous

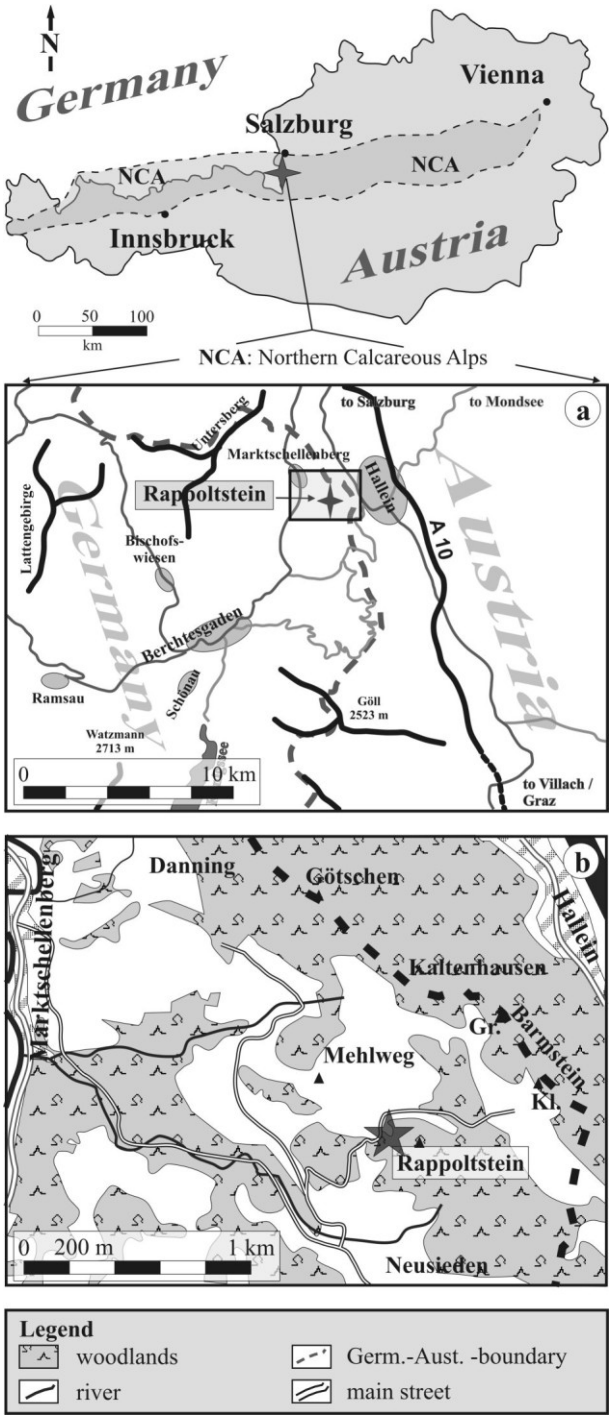

Figure 1: Geography of the study area: (a) overview and (b) detailed map of the Rappoltstein.

Schrambach Formation (Tirolic Nappe) in the west and Carnian red and grey limestones in the east. This infers sharp tectonic boundaries formed by normal faults eastwards and inverse faults westwards. The NNE vergent anticlinal structure of the Rappoltstein (Krystyn and Schlager, 1971) can be also recognised near the outcrop north of the Mehlweg (Fig. 2a): The NNE-fold limb dips uniformly and parallel to the present slope NNE at 47° (Fig. 3c), the SSW fold limb SSW at 25°. The fold axis plunges at 278/10.

3. Methods

The section was sampled bed by bed to obtain conodont data adequate for biozonation. Additionally, the proximity of the locality was mapped in detail (Fig. 3).

Conodont samples (max. 1.5 kg per layer) were dissolved in acetic acid, the insoluble residue was washed and fractioned by sieving (coarse: 250 µm; fine: 100 µm). All selected material is archived at the Institute of Geology and Paleontology, University of Innsbruck (archive Hornung, "Rappoltstein"). All hand samples were etched slightly with acetic acid to see three-dimensional structures. Thin sections provided complementary microfacies data.

Oxygen and carbon stable isotope ratios were measured in all calcareous and marly beds. Due to the absence of articulate brachiopods, three whole-rock powder samples (0.05-0.37 mg) were prepared from every bed using a dental drill. Attention was paid to sample only homogenous mudstones from fresh surfaces without late cements derived from shell cavities or fissure fills (weathered parts were rejected). The powders reacted with phosphoric acid in 10 ml borosilicate extainers after flushing with He. Generated CO_2 was separated from water vapour and was analysed for $\delta^{18}O$ and $\delta^{13}C$ on a GasBench II linked to a Thermo Quest Finnigan Delta^{plus} XL mass spectrometer (Institute for Geology, University of Innsbruck). The results were calibrated against V-PDB. The reproducibility for isotope values was ± 0.13‰ (1s) for $\delta^{18}O$ and ± 0.08 ‰ (1s) for $\delta^{13}C$. For more details see Spötl and Vennemann (2003).

Oxygen isotope analyses of apatite derived from conodonts (sample weight circa 1 mg) were performed on trisilverphosphate by dissolving conodont apatite in nitric acid and precipitating the phosphate group as Ag_3PO_4 (O'Neil et al., 1994). Isotope analysis was performed using a high-temperature conversion-elemental analyzer (TC-EA) linked to a Thermo Finnigan Delta^{plus} mass spectrometer (Institute for Geology, University of Erlangen, Germany). All samples were measured in triplicate. The reproducibility of sample analysis was

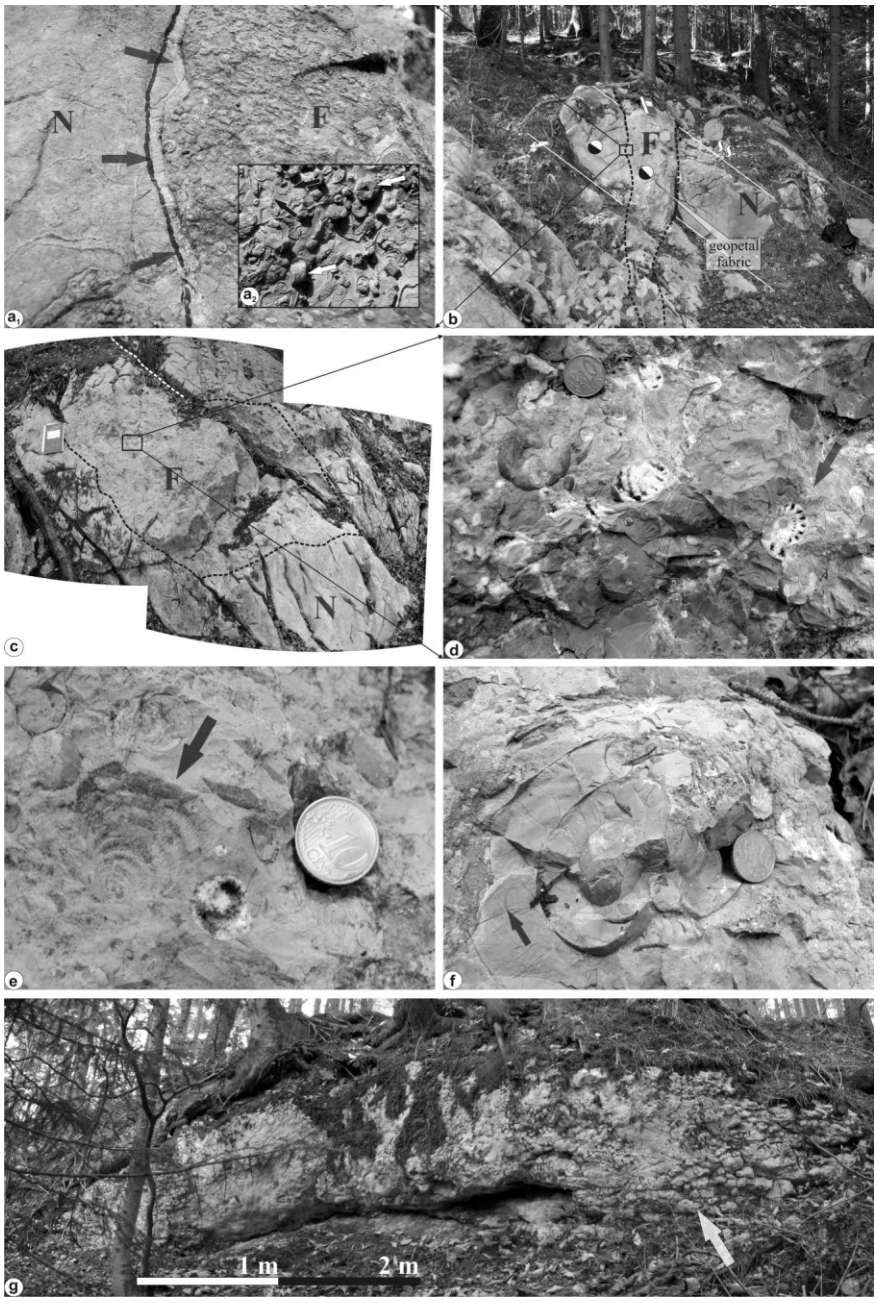

Figure 2: a_1) Radial-fibrous cement seams (large black arrows, thickness ~ 1 cm) mark the distinct boundary between fissure 1 ("F") and host rock ("N") indicating submarine exposure before sedimentary infilling. a_2) Detail of the abundant macrofauna occurring in fissure 1: Crinoid stem ossicles (white arrows) and several cuts through *Cochloceras* sp. (small black arrows). b) Overview of fissure 1. Note the geopetal fabric indicating slight block tilting of the normally bedded host rock before fissure-filling. c) Fissure 3: The black dashed line outlines the distinct borders to the surrounding bioclastic sediment. d) Detail from fissure 2 with faunal components consisting mainly of *Arcestes* sp. e) Imprint of a pectinid bivalve (fissure 3) f) Medium-sized *Arcestes* sp. in fissure 3. g) The nodular and brecciated top of the section (R4) is primary and interpreted as tectonic overprinting due to increased content on marls.

better than ± 0.3 ‰ (1 s). All values are reported in the standard delta notation in permil relative to V-SMOW. Paleotemperatures were calculated using the equation given by Kolodny et al. (1983).

4. Results

4.1. Litho- and Microfacies

Three main lithologic types are differentiated within the section: a) metre-bedded, fossil-poor limestones of grey and red colours, b) a nodular to brecciated horizon on top of the section, and c) red limestones with abundant macrofossils. Following is a short description of these three lithofacies types:

a) The metre-bedded limestones, of grey and red colouring, consist of burrowed biomicritic wacke- to packstones (Figs. 2a, 5a) with rare macrofossils: a few smooth, ss-parallel aligned ammonoids *(Arcestes* sp.) were observed in bed R3. Etched rock surfaces show rare calcified filaments (shells of ?Monotiids or ostracods), juvenile ammonoids and sporadically occurring crinoid stem ossicles. The insoluble residue of the beds R1 to R4 contains textulariid foraminifers (mainly irregular formed *Tolypammina* and planspiral *Ammodiscus*), pyritizised pleurotomariid gastropods, fish teeth (*Saurichthys* sp.) and rare holo-thuroid ossicles (*Theelia* sp.). All beds are completely burrowed. Bored mollusc shells encrusted with mottled, brownish ?algal thrombolites were observed in thin sections (R3; figs. 5b, c). Most of mollusc shells, however, show no encrustation – sporadically occurring dark marginal seams between calcified shells and surrounding micritic matrix are caused by insoluble clayish residues enriched on pressure solution seams. Before stylolitisation, a first diagenetic overprint is observed in thin, mostly vertical tension joints cemented by fine calcite spar. Wider joints as well as solution pores were cemented by coarse blocky calcite spar.

b) The circa 0.7 m thick nodular bed R4 at the top of the section shows abundant ?intraclasts and rounded nodules containing identical fossil contents and sedimentary patterns as described above. The texture is supported by large, centimetre-sized components with only less ochre- to grey coloured clayish, micritic matrix remaining between the lithoclasts and nodules.

c) Red-coloured limestones with abundant macrofossils can be recognised in a sharply bounded zone incising discordantly the above described bioclastic carbonates. The different content of macrofossils, the sharp boundaries to the host rock, and the absence of planar bedding, implies fissures ("Q-fissures" sensu Wendt 1969) which were opened and filled after lithification of the thick limestones. The Rappoltstein section contains three different fissures (Figs. 3a, b).

The main constituent of the macrofauna within the fissure fillings are ammonoids: small tortilicon *Cochloceras* sp. (Figs. 2a$_2$, 5d) and *Arcestes* sp. of variable size (5 to max. 150 mm, see

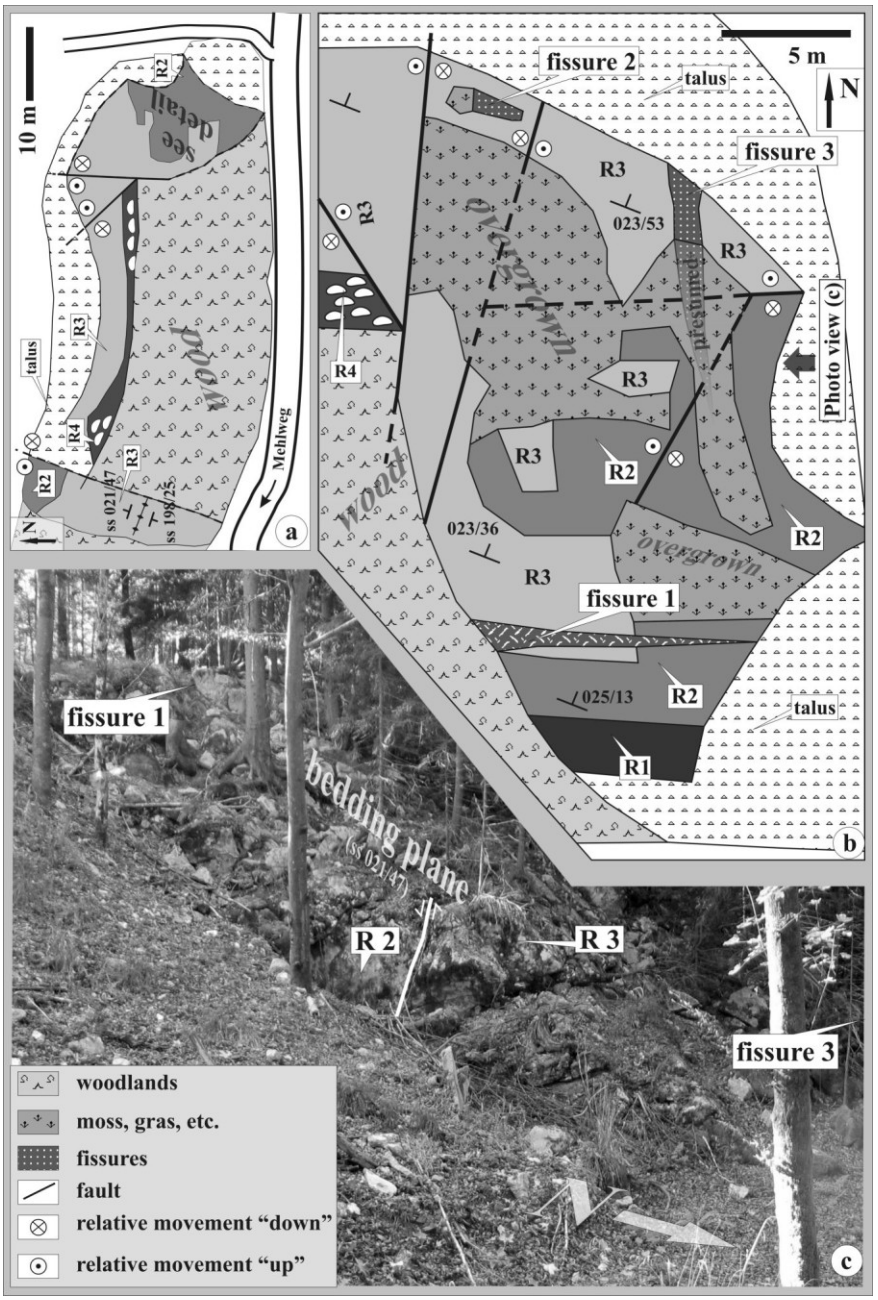

Figure 3: a) Geological map of the outcrop (overview) (b) detailed geological map of the eastern part of the Rappoltstein section with the position of the three fissures. c) Photo of the outcrop.

fig. 2f) dominate in fissure 1. In fissures 2 and 3, solely *Arcestes* sp. was observed. Crinoid stem ossicles are present in all fissures, but occur most abundantly in fissure 1. Some of the ossicles show a slight corrosion. Less common are pectinoid bivalves (fig. 2e) and pleurotomariid gastropods. Insoluble etching residues yielded some textulariid foraminifers.

Nearly all ammonoid shells are aligned chaotically forming a shell-supported framework in a micritic matrix ("ammonoid rudstone"). The ammonite conch diameters range from 20 to 70 mm within fissures 2 and 3, and from 10 to 30 mm in fissure 1. Phragmocon diameters of ca. 100 mm correspond to rare largesized arcestids with a maximum diameter of 175 mm, fig. 2f). Ammonoids may have acted as microfossil traps because their shells are enriched in bioclasts compared to the surrounding micritic matrix, which is rather depleted in small bioclasts < 1 mm (figs. 5d, e, g).

The boundaries of fissures 2 and 3 are not very clear and are defined macroscopically by the sudden increase in the radial-fibrous calcite seams (thickness max. 2 cm). Another peculiarity are thin fractures (up to 2 cm) filled with grey mudstones (S5) cutting through sediment infill of fissure 1 (S3) and disrupting the calcite cement seams (S4) on the walls (Fig. 6).

4.2. Biostratigraphy

The biostratigraphy is based on the local studies of Krystyn (1980). These data are discussed in comparison to the studies of Channell et al. (2003) and Gradstein et al. (2004). All thick-bedded layers (bioclastic wacke- and packstones) yield abundant conodont material adequate for an appropriate biostratigraphical dating.

Because of the long stratigraphic range of *N. steinbergensis* (pl. 1, figs. f-g, i-m) from Alaunian 1 to lowermost Rhaetian (Krystyn 1980), its almost monogeneric occurrence in the bioclastic wacke- and packstones has no biostratigraphic significance. Important is the coexistence with rare *Epigondolella* ex. gr. *bidentata* (Pl. 1, figs. d-e) indicating an approximate assignment into the *bidentata* conodont assemblage zone (A.Z.) representing the uppermost *Halorites macer* and the *Sagenites quinquepunctatus* ammonite zone (Sevatian 1). The coexistence of rare *Misikella hernsteini* (Pl. 1, fig. h) and *Epigondolella* ex gr. *bidentata* (Pl. 1, figs. a-c) found in fissure 2 and fissure 3 without Norigondolellids, however, points to an assignment into the *hernsteini* A. Z. (Gradstein et al., 2004; Kozur and Bachmann, 2005) representing the *Sagenites reticulatus* ammonite zone or the Sevatian 2.

The assemblage of common *N. steinbergensis* and rare *M. hernsteini* found in fissure 1 has, again, no biostratigraphic importance. The presence of abundant *Cochloceras* sp. (fig. 5e), however, indicates another, younger age of sedimentation: According to Channel et al. (2003), the first appearance of *Cochloceras* in Hallstatt Limestones is contemporaneous with the FAD of *Misikella posternsteini* (the successor of *M. hernsteini*) or the Rhaetian base.

All conodonts found within the section show a CAI (Conodont Alteration Index) of 1.0 representing an average thermal overprint of 65° C. The description includes only platform and not ramiform conodonts. The species are shortly described, in order of their first stratigraphical appearance.

A) *Norigondolella steinbergensis* (Mosher, 1968)
(Pl. 1, figs. f, g, i, l, k, m)

1968 *Paragondolella navicula steinbergensis* n. subsp.; in Mosher 1968; Pl. 117, figs. 13, 22
2003 *Norigondolella steinbergensis* (Mosher 1968); in Channell et al. 2003, pl. A3, figs. 22, 23
Material: Abundant, especially in R2 and R3 and fissure 1 (app. 250 complete specimens).
Description: Slightly arcuated and slender specimens. The platform surrounds the posterior denticle from its earliest introduction showing a honeycomb structure on slightly bulged brims with nearly scupltureless troughs inbetween. The large, stepped posterior tooth followed by a saw-blade carina (subadult stages, plate 1, fig. f) or a protracted ridge consisting of affiliated older teeth (hyperadult stages, plate 1, figs. i, k, m). The low anterior carina mostly shows five to seven teeth. Unlike to subadult forms, whose platforms do not extend around the posterior tooth, hyperadult specimens show a posterior platform brim similar to the Lower Norian species *N. navicula* (pers. comm. by L. Krystyn, Vienna,

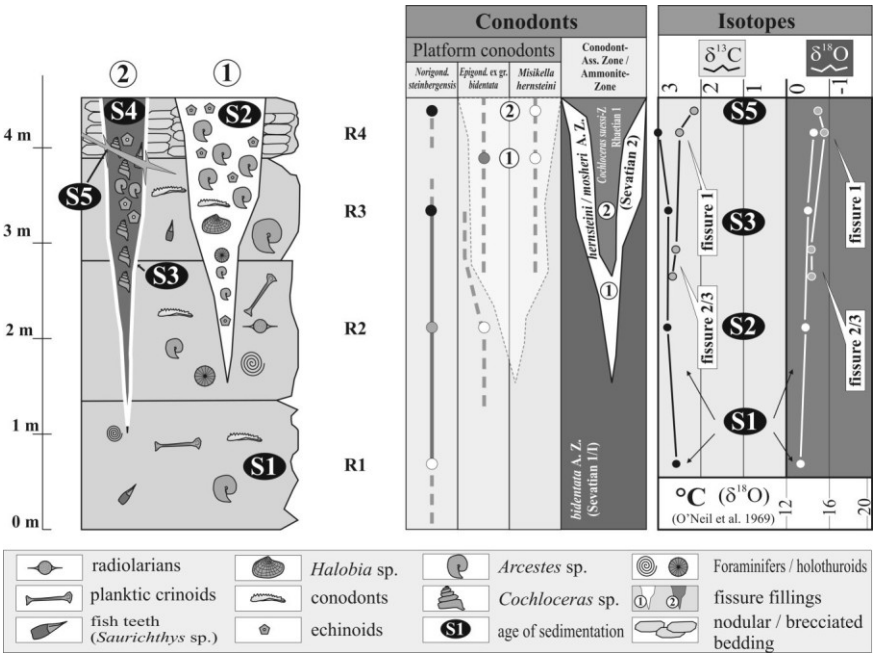

Figure 4: Lithology, content of macrofossils, biostratigraphic zonation and stable isotopes of whole rocks.

and H. Kozur, Budapest). The oval to round basal pit is situated at the posterior end within a broad and bulged circular keel.

Remarks: *N. steinbergensis* originally was described as a new subspecies of "*Paragondolella navicula*" (Huckriede, 1958). According to Krystyn (1980), *N. steinbergensis* has its LAD in the Rhaetian.

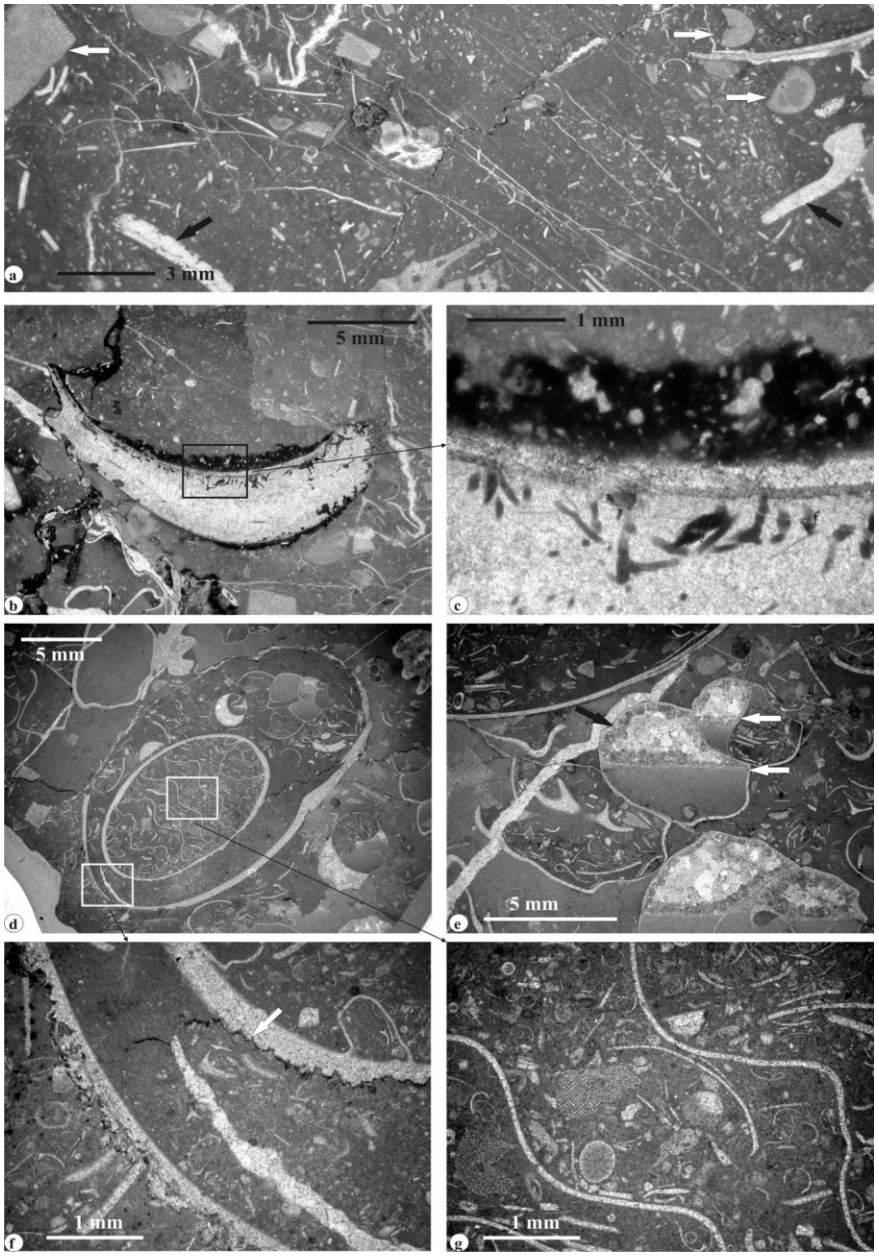

Figure 5: Microfacies of the Hallstatt Limestones from the Rappoltstein section. a) Bioclastic wacke- and packstones with crinoid relics (white arrows), small gastropods (grey arrow) and thick mollusc shells (black arrow) are the most characterising microfacies features of the metre-bedded limestones surrounding the synsedimentary fissures (R3). b) Angular cross-section of a bored and encrusted ?mollusc shell (?algal thrombolites) (R3). c) Detail from a) showing microboring near the shell-surface. d) High concentration of bioclasts in biomolds *(Arcestes* sp.) compared to the surrounding micritic matrix. Note the relatively large-sized *Cochloceras* sp. next to small calcified bioclasts in the upper part of the living chamber (fissure 1). e) *Cochloceras* sp. with well-developed multiple geopetal fabric (white arrows). Note the two different cement generations consisting of marginal fibrous cements (black arrow) and subsequent cemented coarse blocky calcite spar (fissure 1). f) Detail of d) showing pressure solution seams formed due to the competence contrast between micritic matrix and recrystallised shell calcite (white arrow). g) Detail of the ammonite phragmocon from d) and its well-sorted bioclastic filling, which consists of spherical calcified radiolarians, crinoid fragments, small bivalve shells and filaments. The two sinusoidal calcitic lines chamber walls.

B) *Epigondolella* ex gr. *bidentata* Orchard 1991a

(Pl. 1, figs. a-e)

1968 *Epigondolella bidentata*, n. sp.; in Mosher 1968, pl. 118, figs. 31-36

1970 *Epigondolella bidentata* Mosher, 1968; in Mosher 1970; pl. 110, figs. 27-28

1991a *Epigondolella bidentata* Mosher 1968; in Orchard 1991a, fig. 15, pics. Y, W, Z

1991b *Epigondolella bidentata* Mosher 1968; in Orchard 1991b, pl. 12, fig. 4

2003 *Mockina bidentata* (Mosher 1968); in Channel et al. 2003, pl. A3, figs. 7, 9, 27, 41, 42, 50, 51, 56

2003 *Mockina zapfei* (Kozur); in Channel et al. 2003, pl. A2, figs. 53, 55

Material: Rare occurrence in the normal bedded sediment (R3, two specimens), rare in fissure 2 and 3 (three specimens, two fragments).

Description: Small-sized, very slender conodonts with small and reduced platform wearing one single distinct marginal tooth on every side, positioned approximately in mid-length of the prominent carina. The anterior part has five to six highly coalesced teeth, the posterior part four to five distinctive teeth. The slender basal pit is located below the marginal tooth. Microreticulation is completely lacking.

Remarks: Because of the rareness within the section, a possible differentiation between *E. bidentata* and *Mockina zapfei* (a questionable form is pictured in plate 1, fig. a), which is based on the increased space between the teeth, was very difficult. To avoid misclassifications, both conodont species are matched together in the E. bidentata group sensu Orchard, 1991a.

C) *Misikella hernsteini* (Mostler, 1967)

(Pl. 1, fig. h)

1967 *Spathognathodus hernsteini*, n. sp.; in Mostler 1967, pl. 1, figs. 1a-1c

1980 *Misikella hernsteini* (Mostler 1967); in Krystyn 1980; pl. 14, fig. 11

1980 *Misikella hernsteini* (Mostler 1967); in Kovacs and Kozur 1980;

pl. 15, fig. 4, non 5-7
2003 *Misikella hernsteini* (Mostler 1967); in Channell et al. 2003; fig. A3, pics. 57-63
Material: Exclusive, rare occurrence in fissure 2 and fissure 1 (per fissure one sample)
Description: Small-sized specimen with a melted, high carina, six coadunate carinal teeth and a completely reduced platform. The main characteristic is the swelled, oversized drop-shaped and finely serrated basal pit encompassing all teeth except the very anterior one. All carinal teeth are declined in posterior direction, decreasing steadily in size and forming a slightly bended arc. The posterior tooth is declined nearly rectangular relative to the basal plane. The conodont is completely unsculptured.

4.3 Stable Isotopes

Whole rock samples: The average values of isotope ratios are given in Fig. 4. The $\delta^{13}C$ values of bioclastic wacke- and packstones range from 2.6 to 3.0 ‰ V-PDB showing an increasing trend towards the top of the section. The $\delta^{18}O$ values range from -0.4 to -0.7 ‰ showing a clear trend to lighter values towards the top of the section (R4; S1).

The $\delta^{13}C$ values of fissure 2 and 3 plot near the trendline of their surrounding sediment (2.8 ‰), fissure 1 shows lighter values (2.5 ‰). This trend continues into the fine fractures filled with grey mudstones (S5) whose values are lower (2.1 ‰). The $\delta^{18}O$ values of the fissure sediments (-0.6 ‰ for fissures 2 and 3 or S2; -0.8 ‰ for fissure 1 or S3; -0.7 ‰ for S5) deviate from the lower part of the bioclastic wacke- and packstones but approximate towards the upper part of the bioclastic limestones.

Conodont samples: Only the beds R2 and R3 yielded enough conodont material (1 mg) for isotopic measurement. Oxygen isotope ratios of basal Sevatian conodonts (two Norigondolella samples) plot at 22.0 ‰ (V-SMOW) confirming the calculated low palaeotemperatures of whole rock samples (see chapter "discussion"). Due to the low CAI of 1.0, possible diagenetic overprinting can be largely excluded.

5. Discussion

5.1 Genesis of the Rappoltstein synsedimentary fissures

5.1.1 Bedded facies (bioclastic wacke- to packstones) – S1:

Due to the rareness of encrusted mollusc shells (figs. 5b, c) which are thought to indicate hardground conditions and short-termed stratigraphical diastems, the thickly bedded bioclastic wacke- to packstones of the Rappoltstein section are interpreted to have deposited relatively continuously. Both the bedding-parallel aligned ammonoids and the dominantly micritic matrix indicate a low energetic setting without distinct bottoms currents. The intensive burrowing implies a well oxygenated environment and normal aerobic conditions. The nodular and brecciated texture observed at the top of the section (R4) might be a primary feature due to an increased content of marls.

This sedimentary (micro)facies coincides with observations of Krystyn (1991), who described a very similar and age-equivalent facies from the Steinbergkogel near the Hallstatt Lake / Upper Austria, attributing it to the "Hangendrotkalk", a member of the Hallstatt Limestone sequence (sensu Schlager, 1969).

5.1.2 Fissures 2 and 3 (Generation I) – S2:

As described above, the sedimentary filling of fissure 2 and 3 can be approximately dated into Sevatian 2 using conodont biozonation. Long-time submarine exposure may be excluded due to the lack of calcite cement seams lining the fissure margins. Nevertheless, the distinct boundaries of the fissures imply high stability and lithification of the bedrock. The absence of shell encrustations and good preservation of the megafossils indicate not only a quick sedimentary infilling and a rapid sealing with sediment, but also a shortly transported and most probably parautochthonous taphocenosis. Geopetal fabrics measured in both the surrounding bioclastic wacke- to packstones and in the "ammonite rudstone" show identical dip indicating no synsedimentary tilting of the host rock prior to sedimentary infilling.

5.1.3 Fissure 1 (Gene-ration II) S3 – S5:

Unlike the Sevatian fissures, cm-sized radial-fibrous calcite cement seams indicate long-term submarine exposure of fissure

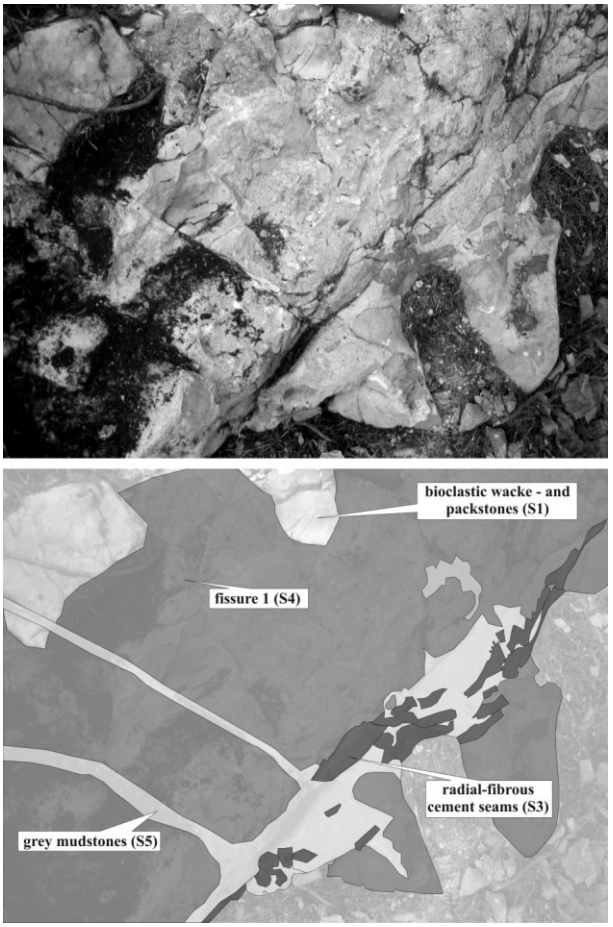

Figure 6: Detail of fissure 1 showing four different ages of sedimentation (S1, S3 – S5).

1 (S3). Their crystal growth points to primary aragonitic seams (?dog tooth cement) recrystallised into calcite. The acute angle of app. 50°, as pictured in fig. 2b, implies high density and lithification of the surrounding bioclastic wacke- and packstones. The interval between opening of the fissure and its sedimentary infilling can be estimated only roughly, but occurred most probably after the opening and filling of fissure-generation 1 (S2) according to the biostratigraphic data. Concerning the growth rate of the aragonite seams, two different hypotheses are conceivable: a) a quick growth rate in a widely opened fissure during submarine exposure without sediment infilling or b) a slow growth rate in a thin fissure fractured locally due to a first tectonic impulse. The second possibility is more likely: the aragonite seams crystallized during cm-sized opening of the fissure – by a second, strong tectonic impulse the fissure dehisced and was then filled rapidly with sediment ("ammonite rudstone" – S4) (Fig. 8).

The sedimentary filling of fissure 1 (S4) can be dated approximately into the Early Rhaetian due to FAD of *Cochloceras* sp. at the Rhaetian base (Channel et al., 2003). The difference of bioclastic content of medium-sized ammonoid shells compared to the surrounding micritic matrix (see figs. 5d, e) might be due to the ammonoid shells acting as "traps" for small-sized fossils during exposure on the bottom. Weak bottom currents transported the shells including their muddy and bioclastic infill into the fissure leading to a chaotic, shell-supported fabric with less micritic matrix (Fig. 7). Rare occurrences of ammonite shells containing no increased bioclastic content, however, may indicate an "active" swimming into the fissure. Abundantly occurring and sporadically corroded crinoid stem ossicles indicate firm- and hardgrounds in the proximity of the fissure (Fig. 7).

Parallel aligned geopetal fabrics within the fissure imply no reworking of semilithified sediment, but rather lithification after the final burial (Fig. 5e). As it can seen in Fig. 2b, the alignments of abundantly occurring geopetal fabrics within the fissure fillings are steeper (~ 10°) than in the bioclastic wacke- and packstones of the host rock (S1) suggesting tectonic related block-tilting during the early Rhaetian (Fig. 8). Another pulse of polyphase synsedimentary movements is documented by thin fractures crossing fissure 1 and disrupting the radial-fibrous calcite seams (S3) (Fig. 6). The joints are filled with fine grey mudstone (S5) and are barren of conodonts. Thus, they can be dated only approximately, but may document the topmost marly limestones of the Hallstatt sequence ("Hangendgraukalk" sensu Schlager, 1969) deposited a short time before the Zlambach marls (Rhaetian 1), which ended the Hallstatt Limestones development (Gawlick, 2000).

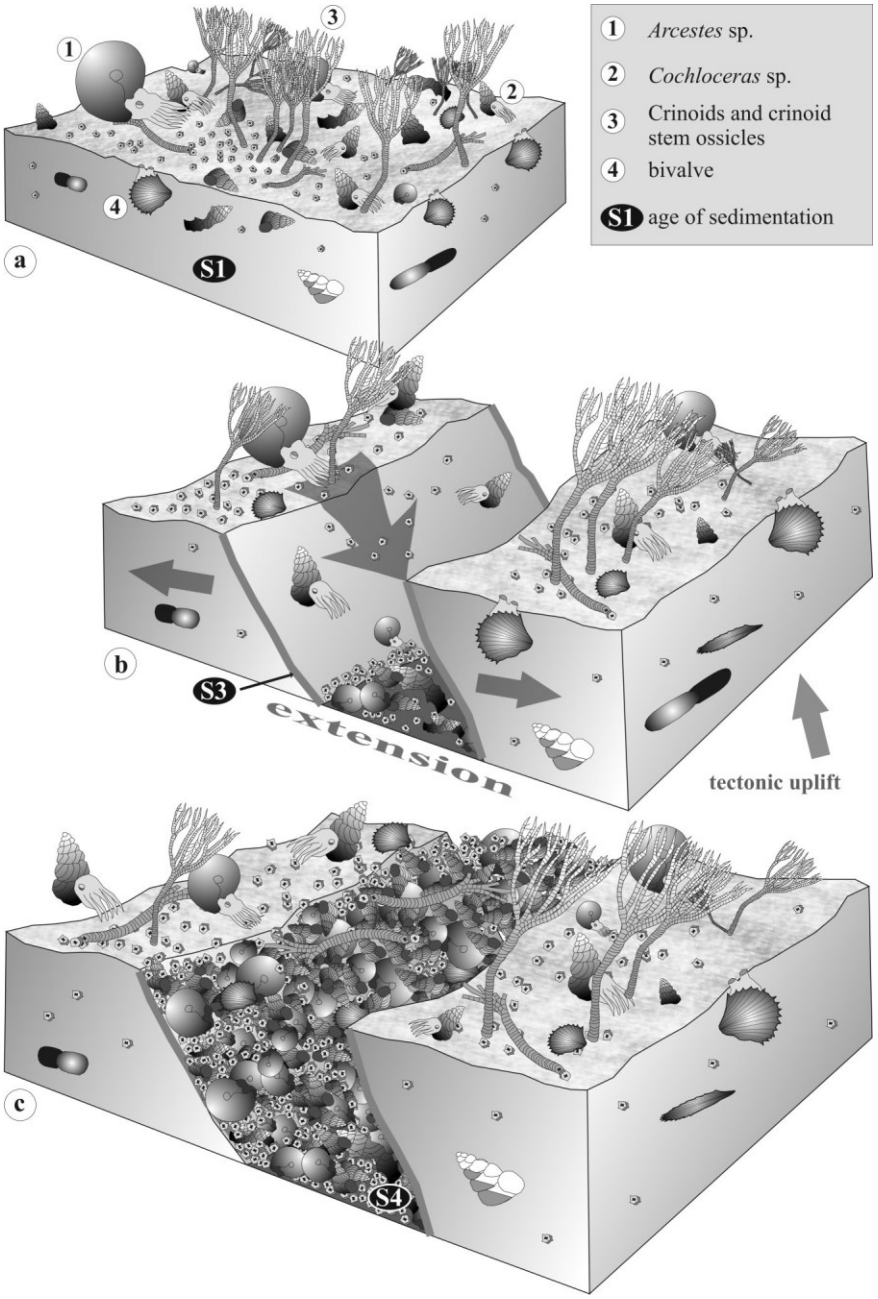

Figure 7: Trophic nucleus of the Rappoltstein *Cochloceras* – *Arcestes*-association as occurring in fissure 1. Rapid tectonical movements caused jointing of the lithified sediments, radial-fibrous aragonite seams crystallized during exposure. The fissure filling reflects an allochthonous / parautochthonous taphocenosis. Modified after Laws (1982).

5.2 Juvavic synsedimentary movements: Triggered by salt diapirism or short-lived tectonic pulses?

According to Schlager (1969), the Hallstatt Limestones were deposited on a starved deep shelf, whose carbonate sequences were fed by the adjacent Wetterstein and Dachstein carbonate platforms (Hornung and Brandner, 2005) but often exhibit subsolution as well as a diminished rate of sedimentation (condensation, hardgrounds). Due to the uniformity of Carnian to Rhaetian depositional spaces, Schlager (1969) assumes a balanced system of the Hallstatt Basin and the shallow marine Wetterstein and Dachstein carbonate platforms. Possible reasons are due to isostatic compensation as indicated by thick carbonate Wetterstein and Dachstein platforms compared to thin basinal Hallstatt successions, but also, according the observations of Schlager (1969) and Mandl (1984, 1999), due to diapiric movements of Upper Permian salt deposits ("Haselgebirge"). These movements are seen as a cause for a narrow-spaced differentiation into basinal areas with marl-related deposits and submarine highs with reduced and pure calcareous sedimentation. Due to the low but uncondensed deposition of the sequence exposed on the northwestern Rappoltstein, it most probably was located on the upper flank of a synsedimentary swell. The sections described by Krystyn (1991) from the Hallstatt region, however, show strong condensation: therefore, their depositional environment would have been located on the ridge-top.

Assuming continuity of salt diapirism and isostatic balance, the extensional movements were most probably not able to generate deep fissures (though Schlager, 1969, documented at other places a discordant penetration of the complete Hallstatt Limestone succession amounting to 80 m). They rather might have been caused by short-lived tectonic pulses occurring locally within the Hallstatt Basin. Obviously, at the Rappoltstein and at the Steinbergkogel (Upper Austria, see Krystyn, 1991), such tectonic pulses occurred contemporaneously in the late Sevatian and at the Rhaetian base. Local tilting, as evidenced in fissure 1 (Fig. 8), might have helped to induce gravitative slope movements and could have triggered the development of the fissures.

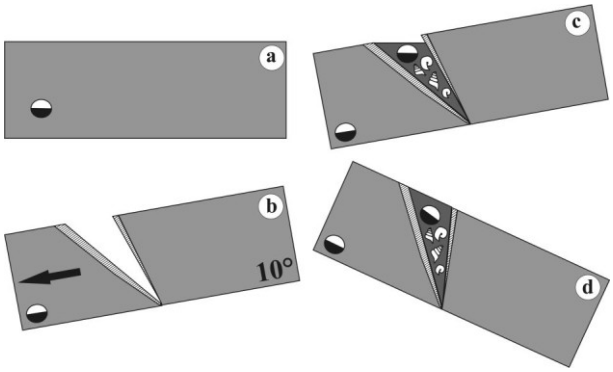

Figure 8: Block-diagrams showing the tectonic development of fissure 1: a) Initial situation, b) opening of the fissure due to gravitate slope movements and growth of aragonite seams, c) sedimentary filling with "ammonite rudstones", d) present situation.

5.3 Isotope record: Evidence for deep water or a cool temperate shallow basin?

5.3.1 Carbon:

The $\delta^{13}C$ values described above are in agreement with the Triassic secular curve of Korte et al. (2005): the authors record a 3,5 ‰-plateau during the Carnian followed by a rapid 1 ‰-drop in the Middle Norian (Alaunian) and a slight decline during the Upper Norian (Sevatian) and Rhaetian. The values presented in table 1, show also a slight decrease from medial 2.8 ‰ in the basal Sevatian to 2.5 ‰ in the Lower Rhaetian (see also fig. 9).

5.3.2 Oxygen:

Calculations carried out on the stable isotope values obtained from whole rock samples (see chapter "results") implicate cold water temperatures ranging from 13,4° to 15,2° C if assuming open marine Triassic seawater $\delta^{18}O$ values close to -1 ‰ V-SMOW or 17.5° to 19,4° C, if assuming values close to 0 ‰ V-SMOW, respectively (table 1). The values for conodont-apatite (table 2) calculated with 12,6° to 12,7° C (-1 ‰ V-SMOW) or 16,9° to 17,1° C (0 ‰ V-SMOW) confirm the whole rock values. Due to the maximum thermal overprint of 65° C (CAI = 1.0), a significant diagenetic alteration of all measured samples can be excluded. Noticeable is the obvious difference between temperatures calculated for the host rock (S1) compared to the fissure fillings: as it can be seen in table 1 and fig. 4, the values for the fissure fillings are more than 0.3 ‰ lighter or 1°C higher than in the surrounding sediment (R1 to R3). This continues the temperature rise which already emerges in the upper part of bioclastic wacke- to packstones (R4).

Palaeotemperatures calculated from whole rock samples, however, may be debatable according to the observation of Gawlick and Böhm (2000): they point out that the instable HM-phase of bulk samples is very instable. Following that, temperatures calculated from whole rock oxygen values may represent not the primary 'real' oceanic signal, but rather temperature and water chemistry during recrystallisation.

According to Joachimski et al. (2004), conodont apatite is an adequate and stable proxy for palaeotemperatures: the two values obtained from monospecific *N. steinbergensis* samples (R2 and R3) result in surprisingly high values of 22.0 ‰ V-SMOW. Supposing that $\delta^{18}O$ values were close to 0 ‰ V-SMOW (present sea-water for ice-house stages, see Korte et al., 2005) and the values reflect 'surface' water temperature, the calculated palaeotemperatures would have ranged within the tolerance of reef building corals (18°-32° C). But assuming that Triassic seawater $\delta^{18}O$ values for ice-free periods were close to -1 ‰ V-SMOW and the hypothesis that the Hallstatt basin reflected water depths of ~ 100 m (e.g. Schlager, 1969; Schmidt, 1990), the determined temperatures from 12.5°C (conodonts) to 15.0° C (whole rocks) would have been very low and not within this tolerance range. This contradicts the fact that, after a phase of widespread Carnian platform demise (e.g. Keim et al., 2001; Hornung and Brandner, 2005), Norian reefs were flourishing again. There are only two possibilities to explain the low

temperatures: a) the Hallstatt Basin was deeper than previously assumed or b) the Hallstatt Basin reflects a relatively shallow basinal environment with significantly colder temperatures, despite the strong affinity to the adjacent carbonate platforms (Hornung and Brandner, 2005). This could be triggered by a cold temperate offshore upwelling zone, which, however, did not reach the reefs. Cold water upstreams might also explain the increasing washout of micritic sediment in direction from the flanks towards the top of the Hallstatt synsedimentary ridges by slight bottom currents. Further, they might have caused strong oxidation as red limestones are typical for the "classical" Hallstatt Limestones successions. However, these points are debatable and will need further studies.

sample	age of sedimentation	biostratigraphic age		$\delta^{13}C$ (‰ V-PDB)	$\delta^{18}O$ (‰ V-PDB)	T (° C) $\delta^{18}O_{sea}$ = -1 ‰	T* (° C) $\delta^{18}O_{sea}$ = 0 ‰
Whole rocks							
R1	S1	Norian	Sevatian 1	2,6	-0,36	13,4	17,5
R2	S1	Norian	Sevatian 1	2,86	-0,43	13,7	17,8
R3	S1	Norian	Sevatian 1	2,78	-0,43	13,4	17,5
R4	S1	Norian	Sevatian 1	3,01	-0,69	13,9	18
Fiss. 2	S2	Norian	Sevatian 2	2,61	-0,63	14,5	18,7
Fiss. 3	S2	Norian	Sevatian 2	2,74	-0,63	14,5	18,7
Fiss. 1	S3	Lower Rhaetian		2,51	-0,81	15,2	19,4
	S5	Lower Rhaetian		2,11	-0,67	14,5	18,7

Table 1: Isotope values of whole rock samples: calculated after O'Neil et al. (1963) & Anderson and Arthur (1983) assuming Triassic sea-water $\delta^{18}O$ values close to -1 ‰ V-SMOW and 0 ‰ V-SMOW, respectively.

sample	age of sedimentation	biostratigraphic age		$\delta^{18}O$ (‰ V-SMOW)	T (° C) $\delta^{18}O_{sea}$ = -1 ‰	T* (° C) $\delta^{18}O_{sea}$ = 0 ‰
Conodonts						
R3	S1	Norian	Sevatian 1	22	12,6	16,9
R4	S1	Norian	Sevatian 1	22	12,7	17,1

Table 2: Isotope values of conodont-apatite: calculated after Kolodny et al. (1983) assuming Triassic sea-water $\delta^{18}O$ values close to -1 ‰ V-SMOW and 0 ‰ V-SMOW, respectively.

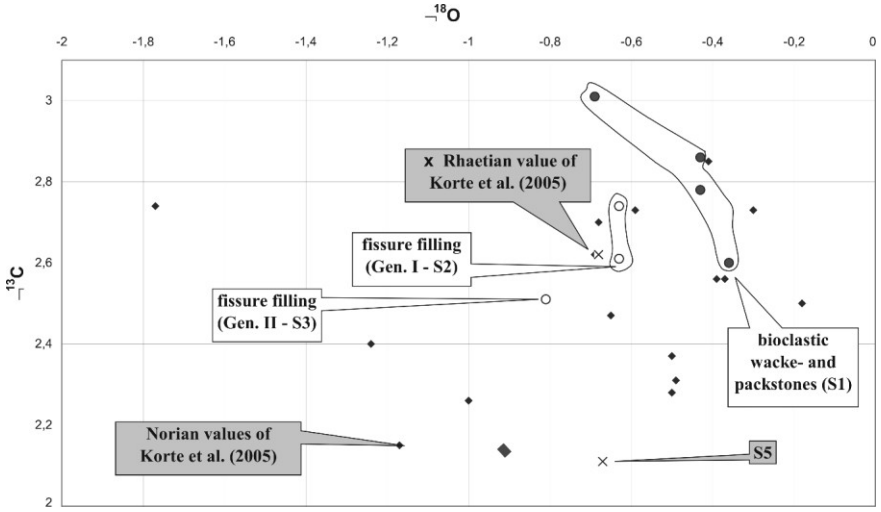

Figure 9: $\delta^{13}C$ / $\delta^{18}O$-crossplot of own isotope data of whole rocks compared to the data of Korte et al. (2005).

6. Conclusions

Multiphase synsedimentary movements causing two different generations of fissures (Sevatian 2 and Rhaetian "ammonite rudstones") and five different stages of sedimentation have penetrated a metre-bedded lower Sevatian Hallstatt Limestone succession exposed at north-western Rappoltstein. Both the "ammonite rudstones" and the surrounding bioclastic sediment were dated using conodonts and ammonoids confirming earlier studies done by Krystyn (1991) in the Hallstatt region (Upper Austria). The generation of the synsedimentary fissures most probably was initiated by both salt diapirism of the underlying Upper Permian Haselgebirge and extensional movements owing to the dispersal and breakup of the supercontinent Pangea. The rupture of the joints happened during short-lived tectonic pulses and/or movements. Isotope data from whole rocks show surprisingly low palaeotemperatures of 14-15° C and a slight temperature increase from Late Norian to Early Rhaetian. Conodonts as good carrier proxies for palaeotemperature provide supplementary oxygen isotope values, which confirm the calculated temperatures obtained from whole rock samples, but even led to the assumption of cool-temperate seawater upstreams in the Hallstatt Basin.

Acknowledgements

Thanks are due to the Austrian Science Fund (FWF) for financial support (P16878). I am sincerely grateful to Antonio Donofrio (Innsbruck), who gave me not only useful hints to conodont determination, but also to the Rappoltstein location. The analytical support of Christoph Spötl (whole rock isotopy; University of Innsbruck) and Michael M. Joachimski (conodont isotopy; University Erlangen-Nuremberg) is appreciated. Further I would like to thank Manuel Rigo (Padua), Heinz Kozur (Budapest) and Leo Krystyn (Vienna) for their advice about conodont taxonomy. Bernard Millen and Monika Tessadri-Wackerle (both Innsbruck) improved the English. The reviews of Wolfgang Schlager (Amsterdam) and Leo Krystyn (Vienna) aided in refining of the ideas presented herein.

References

Anderson, T.F. and Arthur, M.A., 1983. Stable isotopes of oxygen and carbon and their application to sedimentologic and paleoenvironmental problems. In: M.A. Arthur (ed.): Stable Isotopes in Sedimentary Geology. SEPM short course, 10/1 1-151.

Channell, J.E.T., Kozur, H.W., Sievers, T., Mock, R., Aubrecht, R. and Sykora, M., 2003. Carnian-Norian biomagnetostratigraphy at Silicka Brezova (Slovakia): correlation to other Tethyan sections and to the Newark Basin. Palaeogeography, Palaeoclimatology, Palaeoecology, 191, 65-109.

Decker K., Faupl P. and Müller A., 1987. Synorogenic sedimentation on the Northern Calcareous Alps during the Early Cretaceous. In: H.W.Flügel, and P. Faupl (eds.), Geodynamics of the Eastern Alps. Deutike, Wien, 126-141.

Donofrio, D.A., 1975. Mikrofaunistische Untersuchungen der Hallstätter Kalke in den Berchtesgadener Alpen. Unpublished Dissertation University of Innsbruck, 162 pp.

Frank, W., 1987. Evolution of the Austroalpine Elements in the Cretaceous. In: H.W. Flügel and P. Faupl (eds.), Geodynamics of the Eastern Alps. Deutike, Wien, 379-406.

Frisch, W. and Gawlick, H.J., 2003. The nappe structure of the central Northern Calcareous Alps and its disintegration during Miocene tectonic extrusion – a contribution to understanding the orogenic evolution of the Eastern Alps. International Journal of Earth Sciences, 92, 712-727.

Gawlick, H.-J., 2000. Paläogeographie der Obertrias-Karbonatplattformen in den Nördlichen Kalkalpen. Exkursionsführer Sediment 2000. Mitt. Ges. Geol. Bergbaustud. Österr., 44, 46-95.

Gawlick, H.-J., Frisch, W., Vescei, T., Steiger, F. and Böhm, F., 1999. The change from rifting to thrusting in the Northern Calcareous Alps as recorded in Jurassic sediments. Geologische Rundschau 87, 644-657.

Gawlick, H.-J. and Lein, R., 1997. Neue stratigraphische und fazielle Daten aus dem Jakobberg- und Wolfdietrichstollen des Hallein- Bad Dürrnberger Salzberges und ihre Bedeutung für die Interpretation der geologischen Verhältnisse im Bereich der Hallein-Berchtesgadener Schollenregion. Geologisch-Paläontologische Mitteilungen Innsbruck 22, 199-225.

Gawlick, H.-J. and Diersche, V., 2000. Die Radiolaritbecken in den Nördlichen Kalkalpen (hoher Mittel-Jura, Ober-Jura). Exkursionsführer Sediment 2000, Mitteilungen der Gesellschaft geologischer Bergbaustudenten Österreichs, 44, 97-156.

Gawlick, H.-J. and Lein, R., 2000. Die Salzlagerstätte Hallein – Bad Dürrnberg. Exkursionsführer Sediment 2000, Mitteilungen der Gesellschaft geologischer Bergbaustudenten Österreichs., 44, 263-280, Wien.

Gawlick, H.-J. and Böhm, F., 2000. Sequence and isotope stratigraphy of Late Triassic distal periplatform-limestones from the Northern Calcareous Alps (Kälberstein Quarry, Berchtesgaden Hallstatt Zone). Geologische Rundschau, 89, 108-129.

Gradstein, F.M., Ogg, J.G and Smith, A.G., 2005. A geologic time scale 2004. Cambridge University Press, 589 pp.

Gümbel, C.W., 1861. Geognostische Beschreibung des Bayrischen Alpengebirges und seines Vorlandes. Perthes-Verlag, Gotha, 940 pp.

Hornung, T. and Brandner, R., 2005. Biochronostratigraphy of the Reingraben Turnover (Hallstatt Facies Belt): Local black shale events controlled by regional tectonics, climatic change and plate tectonics. Facies 51, 460-479, DOI: 10.1007/s10347-005-0061-x.

Huckriede, R., 1958. Die Conodonten der mediterranen Trias und ihr stratigraphischer Wert. Paläontologische Zeitschrift, 32/3-4, 141-175.

Joachimski, M.M., van Geldern, R., Breisig, S., Buggisch, W. and Day, J., 2004. Oxygen isotope evolution of biogenic calcite and apatite during the Middle and Late Devonian. International Journal of Earth Sciences (Geologische Rundschau), 93, 542-553.

Keim, L., Brandner, R., Krystyn, L. and Mette, W., 2001. Termination of carbonate slope progradation: an example from the Carnian of the Dolomites, Northern Italy. Sedimentary Geology, 143, 303-323.

Krystyn, L., 1980. Triassic conodont localities of the Salzkammergut Region (Northern Calcareous Alps). In: Second European Conodont Symposium-ECOS II, Guidebook and Abstracts. Abhandlungen der Geologischen Bundesanstalt, 35, 61-98.

Krystyn, L., 1991. Die Fossillagerstätten der alpinen Trias. Exkursionsführer, Wien.

Krystyn, L. and Schlager, W., 1971. Der Stratotyp des Tuval. Annales Instituti Geologici Publici Hungarici, 52/2, 591-606.

Krystyn, L., Schäffer, G. and Schlager, W., 1971. Über die Fossillagerstätten in den triadischen Hallstätter Kalken der Ostalpen. Neues Jahrbuch für Geologie und Paläontologie, Abhandlungen 172 (2), 284-304.

Kolodny, Y., Luz, B. and Navon, O., 1983. Oxygen isotope variations in phosphate of biogenic apatites, I. Fish bone apatite - rechecking the rules of the game. Earth and Planetary Science Letters, 64, 398-404.

Korte, C., Kozur, H.W. and Veizer, J., 2005. $\delta^{13}C$ and $\delta^{18}O$ values of Triassic brachiopods and carbonate rocks as proxies for coeval seawater and palaeotemperature. Palaeogeography, Palaeoclimatology, Palaeoecology, 226, 287-306.

Kozur, H. and Bachmann, G., 2005. Correlation of the Germanic Triassic with the international scale. Albertiana, 32, 21-35.

Laws, R.A., 1982. Late Triassic depositional environments and mollsucan associations from west-central Nevada. Palaeogeography, Palaeoclimatology, Palaeoecology, 37:131-148.

Mandl, G.W., 1984. Zur Trias des Hallstätter Raumes – ein Modell am Beispiel Salzkammergut (NKA, Österreich). Mitteilungen der Gesellschaft geologischer Bergbaustudenten Österreichs, 30/31, 133-176.

Mandl, G.W., 1999. The Alpine sector of the Tethyan Shelf – Examples of Triassic to Jurassic sedimentation and deformation from the Northern Calcareous Alps. Mitteilungen der Österreichischen Geologischen Gesellschaft 92, 61-79.

Mojsisovics, E.v., 1893. Die Cephalopoden der Hallstätter Kalke Abhandlungen der Geologischen Reichsanstalt 6 (2), Wien, 835 pp.

Mosher, L.C., 1968. Triassic conodonts from western North America and Europe and their correlation. Journal of Paleontology 42/2, 895-949.

Mosher, L.C., 1970. New conodont species as Triassic guide fossils. Journal. of Paleontology 44/4, 737-742.

Mostler, H., 1967. Conodonten und Holothuriensklerite aus den norischen Hallstätter-Kalken von Hernstein (Niederösterreich). Verhandlungen der Geologischen Bundesanstalt 1 (2), 177-188.

Neubauer, F., 1994. Kontinentkollision in den Ostalpen. Geowissenschaften, 12, 136-140.

O'Neil, J.R., Clayton, R.N. and Mayeda, T.K., 1969. Oxygen isotope fractionation in divalent metal carbonates. Journal of Chemical Physics, 51, 5547-5558.

O'Neil, J.R., Roe, L.J., Reinhard, E. and Blake, R.E., 1994. A rapid and precise method of oxygen isotope analysis of biogenic phosphate. Israel Journal of Earth Science, 43 (3-4), 203-212.

Orchard, M.J., 1991a. Late Triassic conodont biochronology and biostratigraphy of the Kunga Group, Queen Charlotte Islands, British Columbia. In: Woodsworth, G.J. (ed.): Evolution and Hydrocarbon Potential of the Queen Charlotte Basin, British Columbia. Geological Survey of Canada, 90(10), 173-193.

Orchard, M.J., 1991b. Upper Triassic conodont biochronology and new index species from the Canadian Cordillera. In: Orchard, M.J., McCracken (eds.): Ordovician to Triassic Conodont Paleontology of the Canadian Cordillera. Geological Survey of Canada, Bulletin 417, 299-335.

Plöchinger, B., 1955. Zur Geologie des Kalkalpenabschnittes vom Torrener Joch zum Ostfuß des Untersberges; die Göllmasse und die Halleiner Hallstätter Zone. Jahrbuch der Geologischen Bundesanstalt., 95/1, 93-144.

Pichler, H., 1963. Geologische Untersuchungen im Gebiet zwischen Rossfeld und Markt Schellenberg im Berchtesgadener Land. Beihefte des Geologischen Jahrbuches, 48, 129-204.

Schafhäutl, K. E. v., 1848. Über die rothen Ammoniten-Marmore von Oberalm und Adnet in Hinsicht auf die rothen Marmore der bayrischen Voralpen. Neues Jahrbuch für Mineralogie., 1848, 136-148.

Schlager, W., 1969. Das Zusammenwirken von Sedimentation und Bruchtektonik in den triadischen Hallstätterkalken der Ostalpen. Geologische Rundschau, 59, 289-308.

Schlosser, M., 1898. Das Triasgebiet von Hallein. Zeitschrift der deutschen Geologischen Gesellschaft, 50, 333-384.

Schmidt, H., 1990. Mikrobohrspuren in Fossilien der triassischen Hallstätter Kalke und ihre bathymetrische Bedeutung. Facies, 23, 109-120.

Schweigl, J. and Neubauer, F., 1997. Structural evolution of the central Northern Calcareous Alps: Significance for the Jurassic to Tertiary geodynamics in the Alps. Eclogae Geologicae Helvetiae 90, 303-323.

Spötl, C. and Vennemann, T.W., 2003. Continuous-flow isotope ratio mass spectrometer analysis of carbonate minerals. – Rapid Communication Mass Spectrometry 17: 1004-1006.

Wendt, J., 1969. Stratigraphie und Paläogeographie des Roten Jurakalkes im Sonnwendgebirge (Tirol. Österreich). Neues Jahrbuch Geologie und Paläontolgie, Abhandlungen, 132/2, 219-238.

Received: 3. August 2005
Accepted: 20. December 2005

Thomas HORNUNG
Institute for Geology & Palaeontology, Innrain 52, University of Innsbruck, A-6020 Innsbruck.
Email: thomas.hornung@uibk.ac.at

Plate 1:

Conodonts of the Rappoltstein section (scale bar = 100 µm):

Figure A: *Epigondolella* ex gr. *bidentata* Orchard 1991a *(Mockina zapfei* Kozur); upper view – small-sized specimen with short free blade (fissure 2);

Figure B: *Epigondolella* ex gr. *bidentata* Orchard 1991a; upper view; adult specimen with long free blade (fissure 3);

Figure C: *Epigondolella* ex. gr. *bidentata* Orchard 1991a; lateral view (fissure 2);

Figure D: *Epigondolella* ex. gr. *bidentata* Orchard 1991a; upper view; specimen with partly broken platform; note the raised number of posterior and anterior carinal tooths (R3);

Figure E: *Epigondolella* ex. gr. *bidentata* Orchard 1991a; angular view; small specimen with four anterior and three posterior tooths (R3);

Figure F: *Norigondolella steinbergensis* (Mosher 1968); lateral view, subadult specimen with denticled posterior carina, but not extending platform around the posterior tooth (R3);

Figure G: *Norigondolella steinbergensis* (Mosher 1968); lateral view, adult specimen with a low posterior ridge (R3);

Figure H: *Misikella hernsteini;* lateral view (fissure 2);

Figure I: *Norigondolella steinbergensis* (Mosher 1968); angular view; hyperadult growth stage (R3);

Figure K: *Norigondolella steinbergensis* (Mosher 1968); upper view; broken specimen: posterior part without anterior free blade (R3);

Figure L: *Norigondolella steinbergensis* (Mosher 1968); lower view (R3);

Figure M: *Norigondolella steinbergensis* (Mosher 1968); lateral view; hyperadult specimen (R3).

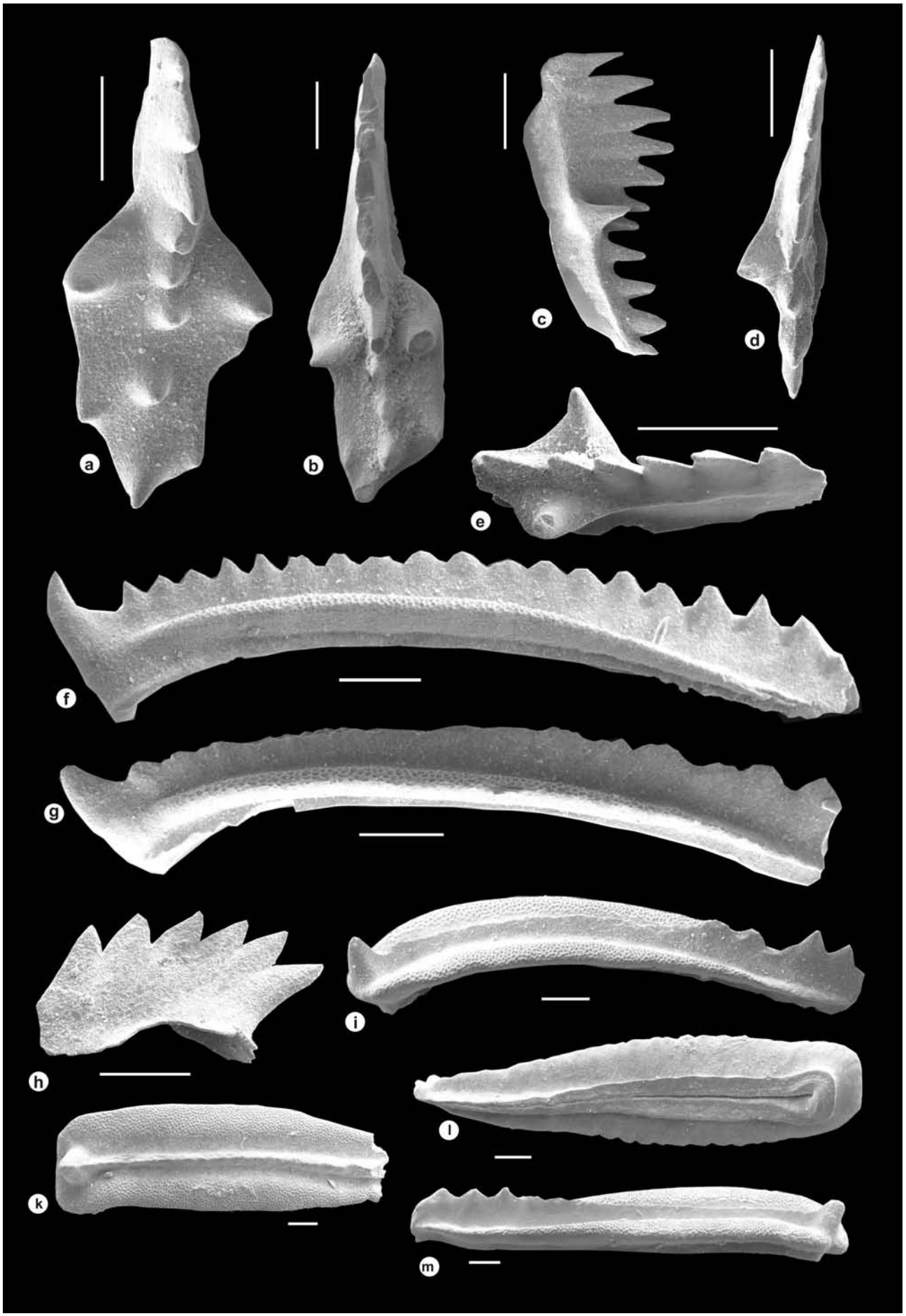
a
b
c
d
e
f
g
h
i
k
l
m